



HAL
open science

Heptacoordinate Structures of Halogenostannanes with Three Phosphine Donors: Significant Influence of Halogen Substituents on Their Geometries

Hajime Kameo, Tatsuya Kawamoto, Shigeyoshi Sakaki, Didier Bourissou,
Hiroshi Nakazawa

► **To cite this version:**

Hajime Kameo, Tatsuya Kawamoto, Shigeyoshi Sakaki, Didier Bourissou, Hiroshi Nakazawa. Heptacoordinate Structures of Halogenostannanes with Three Phosphine Donors: Significant Influence of Halogen Substituents on Their Geometries. *European Journal of Inorganic Chemistry*, 2019, 2019 (26), pp.3045-3052. 10.1002/ejic.201900524 . hal-02398802

HAL Id: hal-02398802

<https://hal.science/hal-02398802>

Submitted on 8 Dec 2019

HAL is a multi-disciplinary open access archive for the deposit and dissemination of scientific research documents, whether they are published or not. The documents may come from teaching and research institutions in France or abroad, or from public or private research centers.

L'archive ouverte pluridisciplinaire **HAL**, est destinée au dépôt et à la diffusion de documents scientifiques de niveau recherche, publiés ou non, émanant des établissements d'enseignement et de recherche français ou étrangers, des laboratoires publics ou privés.

Heptacoordinate Structures of Halogenostannanes with Three Phosphine Donors: Significant Influence of Halogen Substituents on Their Geometries

H. Kameo,* T. Kawamoto, S. Sakaki, D. Bourissou, H. Nakazawa*

Abstract

Structural studies were performed on heptacoordinate compounds of halostannanes $\{(o\text{-Ph}_2\text{P})\text{C}_6\text{H}_4\}_3\text{SnX}$ (X = F (**1**), Cl (**3**), Br (**4**), I (**5**)) with three phosphine donors. The fluorostannane (**1**) has a novel heptacoordinate geometry, in which three phosphine donors interact with the Sn center at the position *trans* to the Sn–F bond (**a** form). In contrast, the chloro (**3**) and bromo (**4**) analogues have a highly distorted pentagonal-bipyramidal geometry (**b** form), and the iodo analogue (**5**) has a tricapped tetrahedral geometry (**c** form). Although both **b** and **c** forms include two phosphine donors coordinating to the Sn center *trans* to the C_{ipso} atoms and one phosphine donor coordinating to the Sn atom at the position *trans* to the halogen atom, the geometry around the Sn center is much more distorted from tetrahedral geometry in **b** form than in **c** form. DFT calculations showed that the presence of the halogen atom at the Sn center facilitated the coordination at the position *trans* to the halogen due to strong electrostatic and charge transfer (CT) interactions and the structural modification by changing the halogen substituent arose from the difference in electronegativity of halogen atom because strongly electronegative halogen enabled the formation of highly distorted structure from tetrahedral geometry (Bent's rule).

Introduction

The chemistry of hypervalent compounds of group 14 elements has been developed due to not only their interesting geometries similar to transition states or intermediates of S_N2 -type reaction but also their essential roles in molecular transformation and catalytic functions.¹ An ER_4 molecule of heavier group 14 element (E) is able to interact with Lewis bases using the $\sigma^*(\text{E}-\text{R})$ orbital to form a hypervalent geometry. The character of heavier group 14 elements causes several and curious geometries involving not only penta- and hexacoordinate structures but also higher coordinate structures.²⁻⁶ These geometries and bonding interactions would be helpful for discussing reaction mechanisms and/or reasons for stereoselectivity. Corriu's group provided several pioneering examples of neutral hepta-coordinate species.² They used a bidentate ligand having 2-electron donor (L) at one end and 1-electron donor (X) at the other end. This type of ligand is denoted as an LX-type ligand hereafter. They reported that silane compounds adopted a heptacoordinate geometry by forming three $\text{LP}(\text{N}) \rightarrow \sigma^*(\text{Si}-\text{X})$ interactions (LP = lone pair) (type I in Chart 1).^{2a} Another type of heptacoordinate silane, germane, and stannane compounds were also investigated by other groups using an L_3X -type ligand (type II).⁴ Both of types I and II form a tricapped tetrahedral geometry around the central atom. Different type of heptacoordinate geometry was reported in stannane systems: the *O,N,N,N,O*-

pentadentate ligands and the combination of *N,N,O*-tridentate and *N,O*-bidentate ligands allowed the formation of pentagonal bipyramidal geometry (type III).⁵

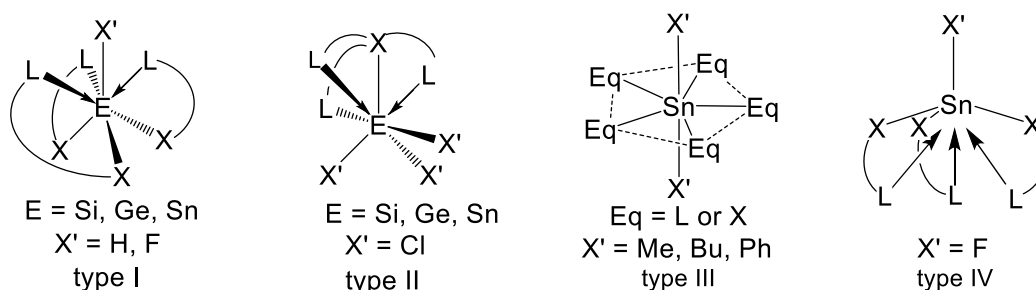


Chart 1. Representative coordination patterns of neutral heptacoordinate species featuring group 14 elements. The caption could be changed for “Representative examples of neutral heptacoordinate species featuring heavier group 14 elements and schematic representation of the associated coordination patterns.”

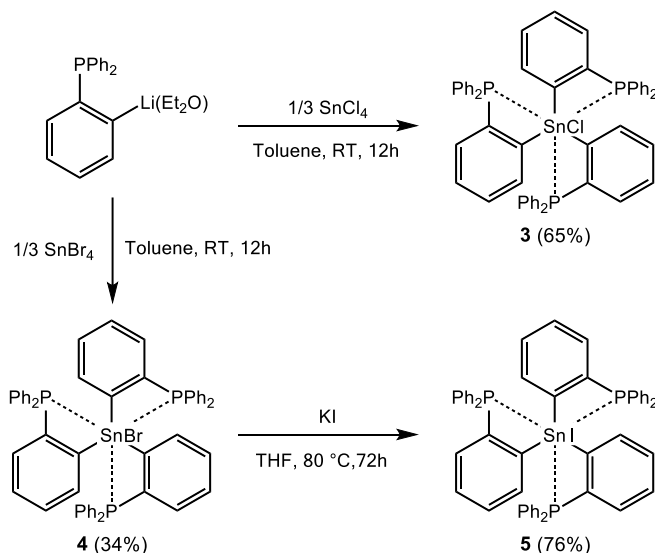
We have been interested in the using a phosphine-based LX-type ligand for the synthesis of novel hypervalent compounds, because strong multiple LP(P)→E charge transfer (CT) interaction is induced by effective overlap between a larger lone pair orbital of phosphine relative to nitrogen donor and a $\sigma^*(\text{E}-\text{X})$ orbital.⁶⁻⁸ Recently, we found that tin fluostannane $\{o\text{-(Ph}_2\text{P)C}_6\text{H}_4\}_3\text{SnF}$ (**1**) adopted an unusual heptacoordinate structure, in which three phosphine donors equivalently interacted with one $\sigma^*(\text{Sn}-\text{F})$ orbital.⁶ FSnC_3 core in **1** strongly distorted from a tetrahedral geometry and its structure adopted a trigonal pyramidal geometry with the axial fluoride atom ($\sum(\text{CSnC}) = 358.23(7)$, $\sum(\text{CSnF}) = 282.96(15)$) (type IV in Chart 1). In contrast, the hydride analogue $\{o\text{-(Ph}_2\text{P)C}_6\text{H}_4\}_3\text{SnH}$ (**2**) of **1** has a different heptacoordinate geometry in which each phosphine donor coordinates via the LP(P)→ $\sigma^*(\text{Sn}-\text{C})$ interactions in a way similar to type I. Note that the HSnC_3 core adopts a less-distorted tetrahedral geometry despite of the presence of P→ $\sigma^*(\text{Sn}-\text{C})$ interactions ($\sum(\text{CSnC}) = 314.86(12)$, $\sum(\text{CSnF}) = 341.1(15)$).

Such unusual hypervalent geometry of **1** motivated us to investigate further on different halogen analogues of **1** for finding different hypervalent structure and elucidating the substituent effect on the heptacoordinate geometry. In this contribution, we performed systematic studies on chloro, bromo, and iodo analogues $\{o\text{-(Ph}_2\text{P)C}_6\text{H}_4\}_3\text{SnX}$ (**3**: X = Cl, **4**: X = Br, **5**: X = I) of **1** and demonstrated that these compounds adopted heptacoordinate geometries which are different from those of **1** and **2**. The origin of these structural modifications was investigated by DFT calculation.

Results and discussions

As ortho-phenylene framework has been reported to be useful for inducing an intramolecular P→Sn

interaction,^{8m} we used this framework for forming three intramolecular P→Sn interactions. The chloro analogue of **1**, *o*-(Ph₂P)₃C₆H₄SnCl (**3**), was isolated by modifying the procedure previously reported.⁹ The reaction of {*o*-(Ph₂P)₃C₆H₄}Li with one third equiv of SnCl₄ provided **3** as a white powder (Scheme 1). The bromo analogue {*o*-(Ph₂P)₃C₆H₄}SnBr (**4**) was successfully synthesized in a way similar to **3** using SnBr₄ instead of SnCl₄. Br/I exchange of **4** using excess amount of KI provided the iodo analogue {*o*-(Ph₂P)₃C₆H₄}SnI (**5**).



Scheme 1. Synthesis of heptacoordinate halostannanes *o*-(Ph₂P)₃C₆H₄}SnX (**3**: X = Cl, **4**: X = Br, **5**: X = I).

X-ray diffraction studies of **3**¹⁰ and **4** were carried out using single crystals obtained from the slow diffusion of n-hexane into dichloromethane solution (Figure 1, Table 1). The structural analysis showed that **3** and **4** had a similar structure but their geometries were different from those of fluoro and hydrido analogues (**1** and **2**). In **3** and **4**, one phosphine donor (P_{ax}) is located at the position *trans* to the halogen X atom, and two phosphine donors (P_{eq}) occupy the position *trans* to *ipso*-carbons, where subscriptions “ax” and “eq” represent axial and equatorial positions, respectively. All Sn–P distances (3.3039(7), 3.4119(7), 3.5087(7) Å for **3**; 3.2688(7), 3.4236(7), 3.5048(7) Å for **4**) are longer than the sum of covalent radii (2.46 Å)¹¹ but significantly shorter the sum of van der Waals radii (4.20 Å),¹² suggesting the presence of P→Sn interaction. Relatively short distance of the Sn–P bond *trans* to the Sn–X bond (X = Cl, Br) is attributed to a strong LP(P_{ax})–σ*(Sn–X) CT interaction. The other two Sn–P bonding interactions are formed by LP(P_{eq})–σ*(Sn–C) CT, but one Sn–P_{eq} distance of ca. 3.41 Å is significantly shorter than the other of ca. 3.51 Å. This is because two phosphine donors *trans* to *ipso*-carbons (P_{eq}) are in different circumstances; one slightly tilts downward and the other tilts upward as shown in Figures 1a and 1c. Accordingly, the lone pairs on the phosphorus atoms tilting upward clearly direct toward the regions of the σ*(Sn–C) orbitals of the Sn center, while that on the

phosphorus tilting downward strays somewhat from the regions of the $\sigma^*(\text{Sn}-\text{C})$ orbitals. As a result, the smaller overlap is found between this LP(P) and $\sigma^*(\text{Sn}-\text{C})$ orbitals, which is responsible for the longer Sn-P distance.

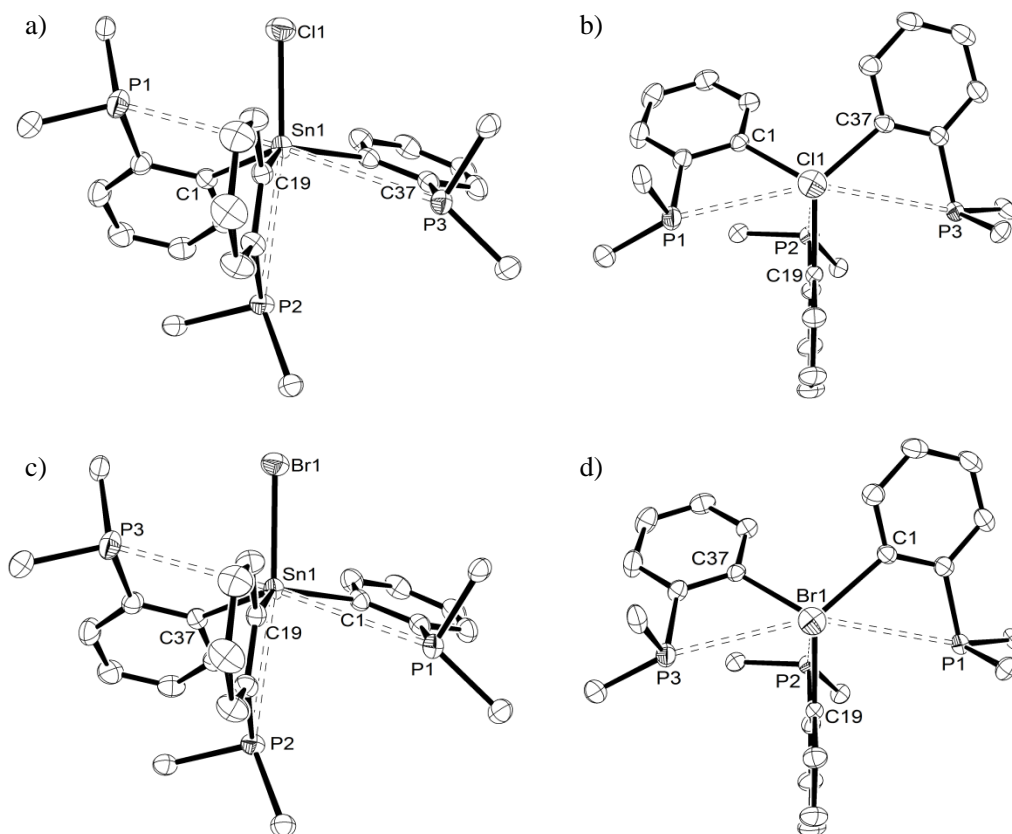


Figure 1. XRD structures of **3** and **4** with thermal ellipsoids set at 40% probability. H atoms and phenyl groups except the *ipso*-carbons are omitted for clarity. a) side view of **3**. b) top view of **3**. c) side view of **4**. d) top view of **4**.

Table 1. Selected Distances (Å) and Angles (°) of **3**, **4** and **5**.

	3 (X = Cl)	4 (X = Br)	5 (X = I)
Sn1-C1	2.148(2)	2.157(3)	2.176(6)
Sn1-C19	2.134(2)	2.136(3)	2.148(6)
Sn1-C37	2.159(2)	2.154(2)	2.181(5)
Sn1-P1	3.4119(7)	3.5048(7)	3.265(2)
Sn1-P2	3.3039(7)	3.2688(7)	3.416(2)
Sn1-P3	3.5087(7)	3.4236(7)	3.4979(18)
Sn1-X	2.3732(7)	2.5255(3)	2.7166(9)
C1-Sn1-C19	112.55(8)	128.59(10)	117.5(2)
C1-Sn1-C37	105.50(9)	105.66(10)	111.3(2)

C19–Sn1–C37	128.53(9)	112.94(9)	110.9(2)
X–Sn–P1	74.75(2)	107.727(14)	157.53(4)
X–Sn–P2	157.89(2)	158.570(16)	80.19(4)
X–Sn–P3	107.73(2)	75.484(16)	78.06(4)

Two Sn–C bonds (2.148(2) and 2.159(2) Å for **3**; 2.154(2) and 2.157(3) Å for **4**) participating in LP(P)– σ^* (Sn–C) interactions are longer than the other (2.134(2) Å for **3**; 2.136(3) Å for **4**), and Sn–X (X = Br, Cl) bonds are slightly longer in **3** and **4** (2.3732(7) Å for **3**; 2.5255(3) Å for **4**) than the corresponding halogenotriphenylstannanes Ph₃SnX (2.360 Å for X = Cl^{13a,13b}; 2.495 Å for X = Br^{13c}), indicating that LP(P)– σ^* (Sn–C) and LP(P)– σ^* (Sn–X) interactions weaken the corresponding Sn–C and Sn–X bonds. The sum of C–Sn–C angles in **3** and **4** are 346.58(15) and 347.19(17), respectively, and C–Sn–X angle in **3** and **4** ranges from 96.47(7) to 108.56(6)°. Also, P_{eq}–Sn–X angles range from 74.8 to 107.7°. Two P_{eq} atoms and three *ipso*-carbons are roughly situated on one plane. P_{ax}–Sn–X angle is considerably large (157.9 for **3**; 158.6° for **4**), indicating that **3** and **4** adopt a pentagonal bipyramidal geometry with P_{ax}–Sn–X axis.

Single crystals of the iodo analogue **5** were prepared from the slow diffusion of n-hexane into the dichloromethane solution. The structure of **5** (Figure 2) is different from those of fluoro (**1**), chloro (**3**) and bromo (**4**) analogues. One phosphine donor (P_{ax}) is located at the position *trans* to the iodo atom, and two phosphine donors (P_{eq}) are situated at the position *trans* to *ipso*-carbons. Although these geometrical features are similar to those of **3** and **4**, both of two phosphine donors *trans* to the *ipso*-carbons tilt downward unlike **3** and **4** (Figure 2a). Accordingly, both of the lone pairs on the phosphorus atoms are directed toward the regions of the σ^* (Sn–C) orbitals, giving rise to a substantially large orbital overlaps between LP(P) and σ^* (Sn–C) orbitals. Three Sn–P distances (3.265(2), 3.416(2), and 3.4979(18) Å) are significantly shorter than the sum of van der Waals radii (4.20 Å),¹² supporting the presence of P→Sn interactions. Similar to **3** and **4**, the Sn–P distance *trans* to the Sn–I bond is the shortest among the three Sn–P distances, which is attributed to the strong LP(P)→ σ^* (Sn–I) CT interaction. Two Sn–C bonds (2.176(6) and 2.181(5) Å) in **5** *trans* to phosphine donors are longer than the other Sn–C bond (2.148(6) Å), and the Sn–I bond (2.7166(19) Å) is somewhat elongated in comparison with that in Ph₃SnI (2.704 Å).¹⁴ These results show the presence of P→ σ^* (Sn–I) and P→ σ^* (Sn–C) interactions. The sum of the three C–Sn–C angles (339.7(3)°) in **5** is significantly less than those of fluoro (**1**), chloro (**3**), and bromo (**4**) analogues, indicating that the SnC₃I core in **5** adopts a less-distorted tetrahedral geometry despite of the presence of LP(P)→ σ^* (Sn–I) and LP(P)→ σ^* (Sn–C) interactions.

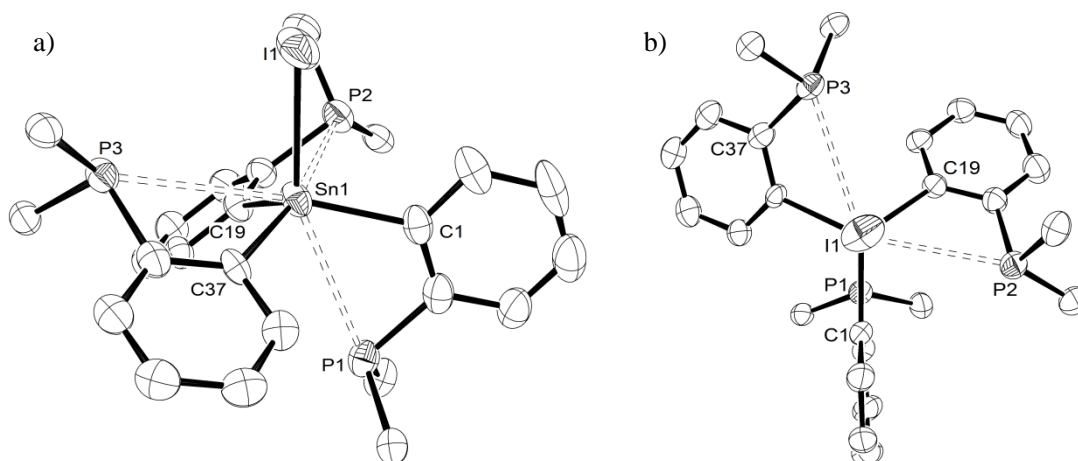


Figure 2. XRD structure of **5** with thermal ellipsoids set at 40% probability. H atoms and phenyl groups except the *ipso*-carbons are omitted for clarity. a) side view. b) top view.

The $^{31}\text{P}\{^1\text{H}\}$ NMR spectrum showed one singlet around 0 ppm ($\delta = -1.2$ ppm ($w_{1/2} = 15.6$ Hz) for **3**; $\delta = -2.2$ ppm ($w_{1/2} = 10.6$ Hz) for **4**; $\delta = -3.1$ ppm ($w_{1/2} = 11.9$ Hz) for **5** in a 4/1 mixture of THF- d_8 and toluene- d_8) (see Figure S1 in ESI). At a low temperature (-80 °C), one broad singlet was observed around 0 ppm ($\delta = -1.5$ ppm ($w_{1/2} = 109.7$ Hz) for **3**; $\delta = -3.7$ ppm ($w_{1/2} = 80.3$ Hz) for **4**; $\delta = -5.3$ ppm ($w_{1/2} = 67.5$ Hz) for **5**), indicating the presence of fast site exchange due to the rotation of *ortho*-diphenylphosphinophenyl groups. Previously, the similar site exchange was reported to undergo more smoothly in $\{o\text{-(Ph}_2\text{P)C}_6\text{H}_4\}_3\text{GeF}$ than in the Si analogue because the longer Ge–C bonds than the Si–C bonds facilitate the rotation of *ortho*-diphenylphosphinophenyl groups.⁷ Similarly, the longer Sn–C bonds are responsible for the faster site exchange in **3** to **5** over NMR time scale. Further, there is a possibility that the presence of an equilibrium including other isomers contributes to the broadening of the signals.

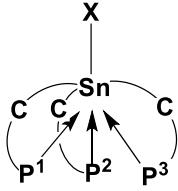
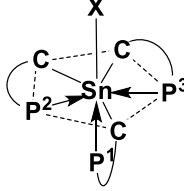
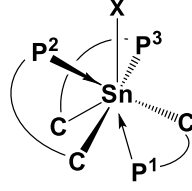
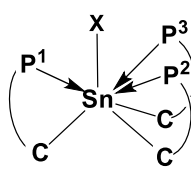
Although the $^{119}\text{Sn}\{^1\text{H}\}$ NMR spectra of **1** and **3** were unavailable due to their low solubility, the $^{119}\text{Sn}\{^1\text{H}\}$ NMR spectra of **4** and **5** provided some information on dative P→Sn interactions. In general, the coordination of organic Lewis bases to stannanes induces a significant high magnetic field shift in ^{119}Sn NMR spectra. Lewis base adducts of Ar_3SnBr bearing a dative N→Sn or O→Sn interaction exhibited ^{119}Sn NMR resonances in the area ranges from -165 to -190 ppm,¹⁵ while the ^{119}Sn NMR signal of Ph_3SnBr is observed at $\delta = -60$ ppm. A large substituent on arene in Ar_3SnBr also induces a high magnetic field shift in the ^{119}Sn NMR spectra (Ar = Ph ($\delta = -60.0$ ppm), Ar = *o*-MeO ($\delta = -74.3$ ppm), Ar = 2,4,6-Me₃C₆H₂: ($\delta = -121.0$ ppm)),¹⁴ although the shift is smaller than that by the coordination of Lewis bases. The chemical shift of **4** ($\delta = -126.6$ ppm) is comparable to that of (2,4,6-Me₃C₆H₂)₃SnBr. In this case, a large shift by strong coordination of Lewis bases was not observed. Similarly, the chemical shift of **5** ($\delta = -177.2$ ppm) is in the range of those of Ar_3SnI (Ar = Ph ($\delta = -113.4$ ppm), Ar = *o*-MeO ($\delta = -135.7$ ppm), Ar = 2,4,6-Me₃C₆H₂: ($\delta = -217.1$ ppm)),¹⁴ and observed

in a lower magnetic field than pentacoordinate species of Ar_3ISnL ($\delta = -230$ to -200 ppm),¹⁶ where L (L = N, O) forms a dative $\text{L}\rightarrow\text{Sn}$ interaction. Therefore, the ^{119}Sn NMR spectra of **4** and **5** indicate that the dative $\text{P}\rightarrow\text{Sn}$ interactions are not very strong although the structural modification can be induced.

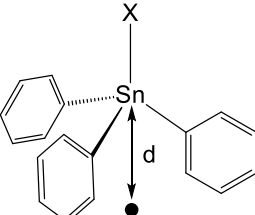
To understand deeply the effect of the halogen substituent in $\{o\text{-(Ph}_2\text{P)C}_6\text{H}_4\}_3\text{SnX}$ (X = F, Cl, Br, I, H) on their geometries, DFT calculations were carried out in a series of heptacoordinate species **1** to **5** and for their possible isomers (four types of geometrical arrangements around the central Sn, **a**, **b**, **c**, and **d** forms) (see Table 2). With **1**, although the **a** form was observed in a solid phase, we obtained the optimized structures of **1a-1d** and evaluated their stabilization energies caused by $\text{LP(P)}-\sigma^*(\text{Sn-X})$ and $\text{LP(P)}-\sigma^*(\text{Sn-C})$ interactions (CT interactions) by DFT calculations. The same optimizations and evaluations were performed for **2-5**. The optimized structures of **3b**, **4b**, and **5c** agreed with the structures obtained by XRD (Table S4 in the ESI). In our previous study, we found that CT and electrostatic interactions played important roles in determining unusual geometry of **1**.⁶ Hence, the electrostatic and CT interactions were firstly investigated.

The sum of $\text{LP(P)}-\sigma^*(\text{Sn-X})$ (X = F, Cl, Br, I, H) and $\text{LP(P)}-\sigma^*(\text{Sn-C})$ CT interactions is listed in Table 2. In halogen systems (**1**, **3-5**), large CT interactions were evaluated in the **a**, **b**, and **c** forms compared with **d** form. The common feature of **a-c** forms is that a phosphine donor is situated at the position *trans* to the Sn-X bond. The largest CT interaction was found in **1c**, **3a**, **4c**, and **5c**. Although **5c** is the most stable, **1c**, **3a**, and **4c** are not the structures observed by XRD. These results indicate that the most stable geometry cannot be rationalized by only CT interaction. Next, we investigated the electrostatic potential at the position *trans* to the Sn-X bond (Figure 3). In the regions *trans* to the Sn-X bond, the electronic potential is more positive in the halogen systems (**1**, **3** to **5**) than in the hydrogen system (**2**). However, the difference among halogen systems is very small, indicating that electrostatic effect is not the main factor for geometrical difference among F, Cl, Br, I compounds.

Table 2. Intramolecular charge-transfer interactions of the lone pair of the phosphine with the σ^* antibonding MOs of Sn–X and Sn–C bonds (kcal/mol).

$\{o-(\text{Ph}_2\text{P})\text{C}_6\text{H}_4\}_3\text{SnX}$	$\sum (\text{LP}(P)-\sigma^*(\text{Sn-X}) \text{ CT} + \text{LP}(P)-\sigma^*(\text{Sn-C}) \text{ CT})$ $P = \text{P}^1, \text{P}^2, \text{P}^3$			
	a form	b form	c form	d form
1 (X = F)	22.5 (1a)	21.3 (1b)	23.8 (1c)	7.0 (1d)
3 (X = Cl)	26.7 (3a)	24.4 (3b)	26.2 (3c)	9.5 (3d)
4 (X = Br)	16.8 (4a)	18.3 (4b)	20.4 (4c)	10.8 (4d)
5 (X = I)	22.5 (5a)	23.4 (5b)	25.5 (5c)	11.8 (5d)
2 (X = H)	6.1 (2a)	10.4 (2b)	11.8 (2c)	11.5 (2d)



d (Å)	X = F	X = Cl	X = Br	X = I	X = H
2.0	+0.102	+0.103	+0.097	+0.095	+0.070
2.5	+0.059	+0.060	+0.056	+0.054	+0.036
3.0	+0.039	+0.040	+0.038	+0.036	+0.023

Figure 3. Electrostatic potential of $\{(o\text{-H})\text{C}_6\text{H}_4\}_3\text{Sn(X)}$ (X = F, Cl, Br, I, H) at the position *trans* to the Sn–X bond.

As CT interactions and electrostatic effect were not able to rationalize the reason why fluoro- (**1**), chloro- (**3**), bromo- (**4**), and iodostannane (**5**) compounds adopt a different structure, we next investigated the effect of electronegative character of halogen atom¹⁷ on sp hybridization of the central Sn. According to Bent's rule, highly electronegative X atom enhances p character of Sn in the Sn–X bond and increases s character of Sn in the Sn–C bond,¹⁸ accordingly causing large C–Sn–C angles. Wharf et al. reported that the s character of Sn in the Sn–C bond in Ph_3SnX (X = F, Cl, Br, I) increases in the order (H) < I < Br < Cl < F through the $^1J_{\text{Sn-C}}$ coupling constant and geometrical features such as the sum of three C–Sn–C angles.^{19,20} These results indicate that higher electronegative halogen is expected to facilitate the formation of a more distorted geometry from a tetrahedral one around the tin center.

As shown in Table 3, the sum of C–Sn–C angles increases in the order **d** form < **c** form < **b** form <

a form, and the average of C–Sn–X angles (X = F, Cl, Br, I, H) decrease in the order **d** form > **c** form > **b** form > **a** form in all systems. These calculation data show that the distortion around the tin center is explained mainly by hybridization of the tin which is caused by X rather than CT interaction and electrostatic effect. The potential energy of Ph₃SnX (X = F, Cl, Br, I, H) was found to strongly depend on the geometric environment around the tin center (Figure 4). For example, the potential energy of Ph₃SnF increases when the average of three C–Sn–F angles (104.7° in optimized geometry of Ph₃SnF) decreases in the order 1.0 kcal/mol (av 100.7°) > 3.7 kcal/mol (av 96.7°) > 8.3 kcal/mol (av 92.7°) > 12.6 kcal/mol (av 90°). Similarly, the potential energy of Ph₃SnX (X = Cl, Br, I, H) increases along with the decrease in the C–Sn–X angles, and the destabilizations increase in the order Ph₃SnF < Ph₃SnCl < Ph₃SnBr < Ph₃SnI < Ph₃SnH. Accordingly, the high electronegative halogen alleviates the destabilization induced by the distortion around the tin atom. This factor would be responsible for the structural modification by changing the halogen substituent.

Table 3. Sum of three C–Sn–C angles and average of three C–Sn–F angles in {*o*-(Ph₂P)C₆H₄}₃SnX (X = F (**1**), Cl (**3**), Br (**4**), I (**5**), H (**2**)) and their isomers.

{ <i>o</i> -(Ph ₂ P)C ₆ H ₄ } ₃ SnX	$\sum (\angle \text{CSnC}),$ average of three C–Sn–F angles			
	a form	b form	c form	d form
1 (X = F)	357.7, 95.0	349.3, 101.1	344.4, 103.3	337.1, 106.4
3 (X = Cl)	356.2, 96.5	348.9, 101.2	341.8, 104.5	335.3, 110.5
4 (X = Br)	355.4, 97.1	343.9, 103.6	338.9, 105.6	321.5, 111.7
5 (X = I)	354.8, 97.6	345.2, 102.9	337.6, 106.1	317.8, 112.8
2 (X = H)	350.5, 100.4	337.2, 106.5	327.7, 109.7	320.2, 112.1

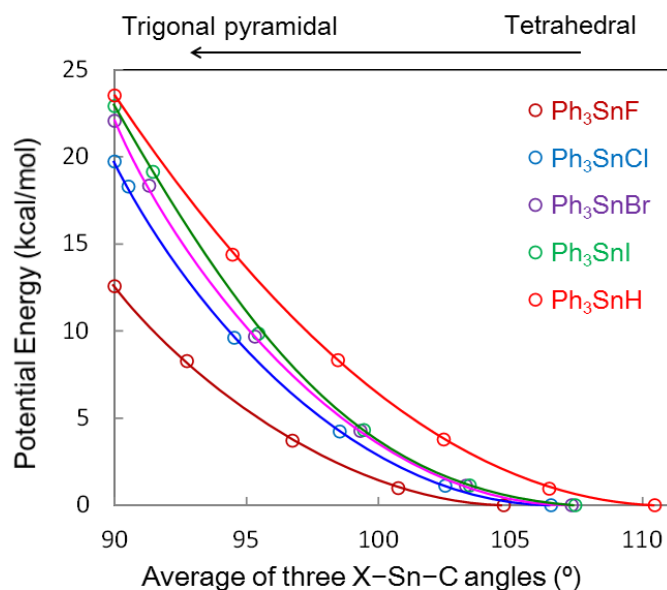


Figure 4. Potential energy of Ph_3SnX ($X = \text{F}, \text{Cl}, \text{Br}, \text{I}, \text{H}$) for which the average C-Sn-X angle in the optimized structure of Ph_3SnX has been progressively diminished to 90° .

In conclusion, we demonstrate the preparation of heptacoordinate bromo- (**4**) and iodostannane (**5**) compounds featuring three $\text{P} \rightarrow \text{Sn}$ interactions. Introduction of a different halogen at the tin center has a noticeable impact on its heptacoordinate geometry. As previously reported, fluorostannane (**1**) adopts a C_3 symmetric geometry, in which three phosphine donors interact with one $\sigma^*(\text{Sn}-\text{F})$ orbital, while the other halogeno analogues adopt a C_1 symmetric geometry. The chloro (**3**) and bromo (**4**) analogues have a distorted pentagonal bipyramidal geometry, and the iodo analogue (**5**) adopts a tri-capped tetrahedral geometry. Geometric alteration appears to be rationalized by the Bent's rule, and the electronegative character of halogen enables the formation of a highly distorted form from tetrahedral geometry.

Experimental Section

General procedures: All experiments were performed under a dry nitrogen atmosphere using standard Schlenk techniques. Benzene- d_6 , toluene- d_8 , tetrahydrofuran- d_8 , and diethylether were dried over sodium benzophenone ketyl and distilled under a dinitrogen atmosphere. Tetrahydrofuran, and *n*-hexane were purified using a two-column solid-state purification system. Chloroform- d and dichloromethane were dried over P_2O_5 and stored over 4-Å molecular sieves. The other reagents used in this study were purchased from commercial sources and used without further purification. ^1H , $^{13}\text{C}\{^1\text{H}\}$ and $^{31}\text{P}\{^1\text{H}\}$ NMR spectra were recorded with a JEOL JNM-AL 400 spectrometer. The ^1H and $^{13}\text{C}\{^1\text{H}\}$ NMR data were analyzed with reference to the residual peaks of the solvent, and $^{31}\text{P}\{^1\text{H}\}$ NMR chemical shifts were referenced to an external 85% H_3PO_4 (0 ppm) sample. Elemental analyses

were conducted using a J-Science Lab JM-10 or FISONs Instrument EA108 elemental analyzer. $\{o\text{-(Ph}_2\text{P)C}_6\text{H}_4\}\text{Li}\cdot\text{Et}_2\text{O}^9$ were prepared as described in the literature.

Preparation of $\{o\text{-(Ph}_2\text{P)C}_6\text{H}_4\}_3\text{Sn}(\text{Cl})$ (3**).** A Schlenk tube was charged with 45.1 μL of SnCl_4 (0.386 mmol) and 5 mL of toluene, and the solution was cooled to $-78\text{ }^\circ\text{C}$. 8 mL toluene solution of $\{o\text{-(Ph}_2\text{P)C}_6\text{H}_4\}\text{Li}\cdot\text{Et}_2\text{O}$ (413 mg, 1.21 mmol) was added slowly to the prepared reaction solution, and the mixture was then allowed to warm to room temperature. The reaction mixture was stirred at ambient temperature for 15 h. After the resulting solution was filtered through a Celite pad, the volatile materials were then removed under reduced pressure to give a white solid. The residue was washed with hexane (5 mL \times 2) and toluene (3 mL \times 2) and dried under vacuum to afford **3** (49.1 mg, 0.0523 mmol) in 14% yield as a white powder. ^1H NMR (400 MHz, C_6D_6): δ 6.86–7.13 (m, 30H), 7.36–7.43 (m, 9H), 8.21–8.24 (m, 3H). $^{31}\text{P}\{^1\text{H}\}$ NMR (163 MHz, C_6D_6): δ -1.4 (s, $J_{\text{P-}^{119}\text{Sn}} = 40.4$ Hz). Anal. Calc. for $\text{C}_{54}\text{H}_{42}\text{ClP}_3\text{Sn}$: C, 69.15; H, 4.51. Found: C, 68.87; H, 4.53.

Preparation of $\{o\text{-(Ph}_2\text{P)C}_6\text{H}_4\}_3\text{Sn}(\text{Br})$ (4**).** A Schlenk tube was charged with 920 mg of $\{o\text{-(Ph}_2\text{P)C}_6\text{H}_4\}\text{Li}\cdot\text{Et}_2\text{O}$ (2.69 mmol) and 10 mL of toluene, and the solution was cooled to $-78\text{ }^\circ\text{C}$. SnBr_4 (115 μL , 0.0876 mmol) was added slowly to the prepared reaction solution, and the mixture was then allowed to warm to room temperature. The reaction mixture was stirred at ambient temperature for 15 h. After the resulting solution was filtered through a Celite pad, the volatile materials were then removed under reduced pressure to give a white solid. The residue was washed with hexane (5 mL \times 2), Et_2O (3 mL), and toluene (2 mL) and dried under vacuum to afford **4** (298 mg, 0.303 mmol) in 34% yield as a white powder. ^1H NMR (400 MHz, CDCl_3): δ 6.92–6.96 (m, 12H, H_{arom}), 7.03–7.09 (m, 12H, H_{arom}), 7.14–7.22 (m, 9H, H_{arom}), 7.30–7.34 (m, 6H, H_{arom}), 7.91–7.94 (m, 3H, H_{arom}). $^{13}\text{C}\{^1\text{H}\}$ NMR (100 MHz, CDCl_3): δ 128.2 (s), 128.2 (m), 129.0 (m), 129.7 (s), 133.3 (m), 135.2 (2), 137.5 (m), 138.0 (m), 143.5 (s), 156.1 (m). $^{31}\text{P}\{^1\text{H}\}$ NMR (162 MHz, CDCl_3): δ -1.3 (s, $^1J_{\text{F-}^{119}\text{Sn}} = 60.5$ Hz). $^{119}\text{Sn}\{^1\text{H}\}$ NMR (187 MHz, CDCl_3): δ -126.6 (s, $^1J_{\text{P-}^{119}\text{Sn}} = 46.9$ Hz). Anal. Calc. for $\text{C}_{54}\text{H}_{42}\text{BrP}_3\text{Sn}$: C, 66.02; H, 4.31. Found: C, 66.18; H, 4.49.

Preparation of $\{o\text{-(Ph}_2\text{P)C}_6\text{H}_4\}_3\text{Sn}(\text{I})$ (5**).** A Schlenk tube was charged with 152 mg of $\{o\text{-(Ph}_2\text{P)C}_6\text{H}_4\}_3\text{SnBr}$ (0.155 mmol), 924 mg of KI (5.57 mmol), and 15 mL of THF, and the reaction mixture was stirred at $80\text{ }^\circ\text{C}$ for 72 h. The volatile materials were then removed under reduced pressure, and the residue was extracted with benzene. After the solution was filtered through a Celite pad, the volatile materials were then removed under reduced pressure to give a white solid. The residue was washed with hexane (5 mL \times 2) and dried under vacuum to afford **5** (121 mg, 0.118 mmol) in 76% yield as a white powder. ^1H NMR (400 MHz, CDCl_3): δ 6.92–6.98 (m, 12H, H_{arom}), 7.07–7.11 (m, 12H, H_{arom}), 7.14–7.22 (m, 9H, H_{arom}), 7.25–7.29 (m, 6H, H_{arom}), 7.91–7.94 (m, 3H, H_{arom}). $^{31}\text{P}\{^1\text{H}\}$ NMR

(162 MHz, CDCl₃): δ -1.7 (s, $^1J_{F-^{119}\text{Sn}} = 55.0$ Hz). $^{119}\text{Sn}\{^1\text{H}\}$ NMR (187 MHz, CDCl₃): δ -177.2 (s, $^1J_{P-^{119}\text{Sn}} = 64.6$ Hz). $^{13}\text{C}\{^1\text{H}\}$ NMR (100 MHz, CDCl₃): δ 128.1 (s), 128.3 (t, $J_{P-C} = 13.2$ Hz), 129.4 (m), 129.7 (d, $J_{P-C} = 5.8$ Hz), 133.4 (m), 135.2 (s), 137.4 (m), 138.5 (m), 143.4 (s), 154.2 (m). Anal. Calc. for C₅₄H₄₂IP₃Sn: C, 63.00; H, 4.11. Found: C, 62.74; H, 4.30.

Structure Determination by X-ray Diffraction. Single crystals suitable for X-ray diffraction analysis were obtained as described above. Diffraction intensity data were collected with a Rigaku/MSC Mercury CCD diffractometer at 200 K(2), and a semiempirical multi-scan absorption²¹ correction was performed. The space groups were chosen based on the systematic absences in the diffraction data. The structures were solved using SIR97²² by subsequent difference Fourier synthesis, and refined by full matrix least-squares procedures on F^2 . All non-hydrogen atoms were refined with anisotropic displacement coefficients. The hydrogen atoms were treated as idealized contributions and refined in rigid group model. All software and sources of scattering factors are contained in the SHELXL97 program package.²³ CCDC 1425640, 1425641, and 1425642 contain supplementary crystallographic data for this paper. These data can be obtained free of charge from the Cambridge Crystallographic Data Centre via www.ccdc.cam.ac.uk/data_request/cif.

Density Functional Theory Calculations. Gaussian09 was employed for all calculations here.²⁴ The geometry was optimized by the DFT method with the M06²⁵ functional in C_1 symmetry. For Sn and I atom, the Stuttgart–Dresden–Born (SDD) basis set²⁶ attaching two additional d polarization functions²⁷ was used with the corresponding effective core potentials (ECPs). Usual 6-311G(d,p) basis sets were employed for C, H, P, and usual 6-311+G(d,p) basis sets were employed for F, Cl, Br. Key geometric data for **3b**, **4b**, and **5c** agreed with the experimental values in the solid state (see Table S9 in the SPI).

ACKNOWLEDGMENT

This research was supported by a Challenging Exploratory Research grant (No. 15K13662) and a Grant-in-Aid for Scientific Research on Innovative Areas “Stimuli-Responsive Chemical Species” (No. 15H00957) from MEXT. H.K. acknowledges the financial support from the Kyoto Technoscience Center and a Grant-in-Aid for Scientific Research (C) (No. 15K05458). S.S. wishes to acknowledge the support from the Ministry of Education, Culture, Science, Sport and Technology through Grants-in-Aid of Specially Promoted Science and Technology (No. 22000009) and Japan Science and Technology Cooperation (CREST ‘Establishment of Molecular Technology towards the Creation of New Functions’ Area).

References

1. (a) Akiba, K.-y. in *Chemistry of Hypervalent Compounds*, John Wiley & Sons: New York, **1999**. (b) Baukov, Y. I.; Tandura, S. N. *Hypervalent Compound of Organic Germanium, Tin and Lead derivatives*; in *The chemistry of Organic Germanium, Tin and Lead Compounds*, Vol. 2 (Ed.: Rappoport, Z.), Wiley, Chichester, **2002**, pp. 963. (c) Kost, D.; Kalikhman, I. *Hypervalent Silicon Compounds*; in *The Chemistry of Organic Silicon Compounds*, Vol.2 (Eds.: Rappoport, Z.; Apeloig, Y.), Wiley, New York, **1998**, pp. 1339. (d) Brook, M. A. in *Silicon in Organic, Organometallic, and Polymer Chemistry*, John Wiley & Sons: New York, **2000**. pp. 97.
2. (a) Brelière, C.; Carré, F.; Corriu, R. J. P.; Royo, G. *Organometallics* **1988**, *7*, 1006. (b) Carré, F.; Chuit, C.; Corriu, R. J. P.; Mehdi, A.; Reyé, C. *Angew. Chem. Int. Ed. Engl.* **1994**, *33*, 1097 (c) Brelière, C.; Carré, F.; Corriu, R. J. P.; Royo, G.; Man, M. W. C. *Organometallics* **1994**, *13*, 307. (d) Carré, F.; Chuit, C.; Corriu, R. J. P.; Fanta, A.; Mehdi, A.; Reyé, C. *Organometallics* **1995**, *14*, 194.
3. (a) Auner, N.; Probst, R.; Hahn, F.; Herdweck, E. *J. Organomet. Chem.* **1993**, *459*, 25. (b) Kawachi, A.; Tanaka, Y.; Tamao, K. *Organometallics* **1997**, *16*, 5102.
4. (a) Dostal, S.; Stoudt, S. J.; Fanwick, P.; Sereatan, W. F.; Kahr, B.; Jackson, J. E. *Organometallics* **1993**, *12*, 2284. (b) Kobayashi, J.; Ishida, K.; Kawashima, T. *Silicon Chem.* **2002**, *1*, 351. (c) Iwanaga, K.; Kobayashi, J.; Kawashima, T.; Takagi, N.; Nagase, S. *Organometallics* **2006**, *25*, 3388.
5. (a) Ramírez-Jiménez, A.; Gómez, E.; Hernández, S. *J. Organomet. Chem.* **2009**, *694*, 2965. (b) González, A.; Gómez, E.; Cortés-Lozada, A.; Hernández, S.; Ramírez-Apan, T.; Nieto-Camacho, A. *Chem. Pharm. Bull.* **2009**, *1*, 5.
6. H. Kameo, T. Kawamoto, S. Sakaki, H. Nakazawa *Organometallics* **2014**, *33*, 5960-5963.
7. H. Kameo, T. Kawamoto, D. Bourissou, S. Sakaki, H. Nakazawa *Organometallics* **2014**, *33*, 6557-6567.
8. Examples of hypervalent group 14 element compounds with phosphorous donor are limited even in hepta- and hexacoordinate species. See (a) A. Tzschach, k. Jurkschat, *Comm. Inorg. Chem.* **1983**, *3*, 35-50. (b) H. Weichmann, *J. Organomet. Chem.* **1984**, *262*, 279. (c) H. Weichmann, J. Menuhier-Pier, M. van Meerssche, *J. Organomet. Chem.* **1986**, *309*, 267. (d) K. Jurkschat, Z. Tzschach, H. Weichmann, P. Rajczy, M. A. Mostafa, L. Korecz, K. Burger, *Inorg. Chim. Acta* **1991**, *179*, 83. (e) Grobe, J.; Hildebrandt, W.; Martin, R.; Walter, A. *Z. Anorg Allg Chem* **1991**, *592*, 121. (f) S. Hoppe, H. Weichmann, K. Jurkschat, C. Schneider-Koglin, M. Dräger, *J. Organomet. Chem.* **1996**, *505*, 63. (g) H. H. Karsch, B. Deubelly, U. Keller, F. Bienlein, R. Richter, P. Bissinger, M. Heckel, G. Muller, *Chem. Ber.* **1996**, *129*, 759-764. (h) U. Baumeister, H. Hartung, A. Krug, K. Merzweiler, T. Schulz, C. Wagner, H. Weichmann, *Z. Anorg. Allg. Chem.* **2000**, *626*, 2185. (i) K. A. Clark, T. A. George, T. J. Brett, C. R. Ross, II, R. K. Shoemaker, *Inorg. Chem.* **2000**, *39*, 2252-2253. (j) C. H. Yoder, L. A. Margolis, J. M. Horne, *J. Organomet. Chem.* **2001**, *633*, 33. (k) Toshimitsu, A.; Saeki, T.; Tamao, K. *J. Am. Chem. Soc.* **2001**, *123*, 9210. (l) Quintard, D.; Keller, M.; Breit, B. *Synthesis* **2004**, 905. (m) Lin, T.-P.; Gualco, P.; Ladeira, S.; Amgoune, A.; Bourissou, D.; Gabbaï, F. P. C. *R. Chim.* **2010**, *13*, 1168. (n) Sanji, T.;

- Naito, K.; Kashiwabara, T.; Tanaka, M. *Heteroatom Chem.* **2012**, *23*, 520-524. (o) H. Kameo, H. Nakazawa, R. H. Herber, *J. Mol. Struct.* **2013**, *1054-1055*, 321-325.
9. H. Kameo, S. Ishii, H. Nakazawa. *Organometallics*, **2012**, *31*, 2212-2218.
10. Although we previously reported the structural data for $\{(o\text{-Ph}_2\text{P})\text{C}_6\text{H}_4\}_3\text{Sn}(\text{Cl})$ (**3**), the presence of three P→Si interactions was not demonstrated.⁹ In this contribution, we discuss on its structure using crystal data of better crystals
11. Cordero, B.; Gómez, V.; Platero-Prats, A. E.; Revés, M.; Echeverría, J.; Cremades, E.; Barragán, F.; Alvarez, S. *Dalton Trans.* **2008**, *37*, 2832.
12. Batsanov, S. S. *Inorg. Mater.* **2001**, *37*, 871.
13. (a) J. S. Tse, F. L. Lee, E. J. Gabe, *Acta Crystallogr. Sect. C* **1986**, *42*, 1876. (b) S. W. Ng, *Acta Crystallogr. Sect. C* **1995**, *51*, 2292. (c) H. Preut, F. Huber, *Acta Crystallogr. Sect. B* **1979**, *35*, 2292.
14. (a) M.G. Simard, I. Wharf, *Acta Crystallogr. Sect. C* **1994**, *50*, 397. (b) S.W. Ng, *Acta Crystallogr. Sect. C* **1995**, *51*, 629.
15. (a) G. Koten, J. Jastrzebski, J. Boersma, P. Esch, *Organometallics* **1991**, *10*, 930. (b) G. Koten, J. Jastrzebski, J. Boersma, *J. Organomet. Chem.* **1991**, *413*, 43. (c) M. Mehring, C. Low, M. Schurmann, K. Jurkschat, *Eur. J. Inorg. Chem.* **1999**, *5*, 887.
16. (a) C. Silvestru, R. Varga, A. Rotar, M. Schurmann, K. Jurkschat, *Eur. J. Inorg. Chem.* **2006**, *7*, 1475. (b) P. Cmoch, D. Matkowska, M. Gola, M. Sniezek, K. Stalinski *J. Organomet. Chem.* **2007**, *692*, 2036.
17. Allred-Rochow electronegativities of halogen atoms; F: 4.10, Cl: 2.83, Br: 2.74, I:2.21.
18. (a) Weinhold, F.; Landis, C. L. *Valency and Bonding: A Natural Donor-Acceptor Perspective*, Cambridge University Press, Cambridge, **2005**, pp. 138. (b) Bent, H. A. *Chem. Rev.* **1961**, *61*, 275-311.
19. Wharf, I.; Lebuis, A.-M.; Roper, G. A. *Inorg. Chim. Acta*, **1999**, *294*, 224.
20. DFT calculations indicate that the sum of C-Sn-C angles in Ph₃SnX (X = F, Cl, Br, I, H) significantly smaller in hydrido system H (325.3) than halogen systems (336.0-341.3), implying that the steric factor makes little influence on the distortion around the tin atom .
21. Rigaku. REQAB. Version 1.1. Rigaku Coporation, Tokyo, Japan, **1998**.
22. Altomare, A.; Burla, M. C.; Camalli, M.; Cascarano, G.; Giacovazzo, C.; Guagliardi, A.; Moliterni, A. G. G.; Spagna, *J. Appl. Crystallogr.*, **1999**, *32*, 115.
23. G. M. Sheldrick, SHELXL97: Program for the Refinement of Crystal Structures, University of Göttingen, Germany, **1997**.
24. Frisch, M. J.; Trucks, G. W.; Schlegel, H. B.; Scuseria, G. E.; Robb, M. A.; Cheeseman, J. R.; Scalmani, G.; Barone, V.; Mennucci, B.; Petersson, G. A.; Nakatsuji, H.; Caricato, M.; Li, X.; Hratchian, H. P.; Izmaylov, A. F.; Bloino, J.; Zheng, G.; Sonnenberg, J. L.; Hada, M.; Ehara, M.; Toyota, K.; Fukuda, R.; Hasegawa, J.; Ishida, M.; Nakajima, T.; Honda, Y.; Kitao, O.; Nakai, H.;

- Vreven, T.; Montgomery, Jr., J. A.; Peralta, J. E.; Ogliaro, F.; Bearpark, M.; Heyd, J. J.; Brothers, E.; Kudin, K. N.; Staroverov, V. N.; Kobayashi, R.; Normand, J.; Raghavachari, K.; Rendell, A.; Burant, J. C.; Iyengar, S. S.; Tomasi, J.; Cossi, M.; Rega, N.; Millam, N. J.; Klene, M.; Knox, J. E.; Cross, J. B.; Bakken, V.; Adamo, C.; Jaramillo, J.; Gomperts, R.; Stratmann, R. E.; Yazyev, O.; Austin, A. J.; Cammi, R.; Pomelli, C.; Ochterski, J. W.; Martin, R. L.; Morokuma, K.; Zakrzewski, V. G.; Voth, G. A.; Salvador, P.; Dannenberg, J. J.; Dapprich, S.; Daniels, A. D.; Farkas, Ö.; Foresman, J. B.; Ortiz, J. V.; Cioslowski, J.; Fox, D. J. *Gaussian09*, Gaussian, Inc., Wallingford CT, **2009**.
25. Zhao, Y., Truhlar, D. G. *Theor. Chem. Acc.* **2008**, *120*, 215.
26. Dolg, M.; Stoll, H.; Preuss, H.; Pitzer, R. M. *J. Phys. Chem.* **1993**, *97*, 5852.
27. Martin, J. M. L.; Sundermann, A. *J. Chem. Phys.* **2001**, *114*, 3408.

Hepta-coordination

